Applied Catalysis B: Environmental 254 (2019) 47–54

Contents lists available at ScienceDirect

Applied Catalysis B: Environmental

journal homepage: www.elsevier.com/locate/apcatb

Powerful uranium extraction strategy with combined ligand complexation and photocatalytic reduction by postsynthetically modified photoactive metal-organic frameworks

Hui Li[a], Fuwan Zhai[b,c], Daxiang Gui[b], Xiangxiang Wang[b], Chunfang Wu[b], Duo Zhang[b], Xing Dai[b], Hong Deng[a], Xintai Su[a], Juan Diwu[b], Zhang Lin[a,*], Zhifang Chai[b], Shuao Wang[b,*]

[a] School of Environment and Energy, Key Laboratory of Pollution Control and Ecosystem Restoration in Industry Clusters (Ministry of Education), South China University of Technology, Guangzhou 510006, China
[b] State Key Laboratory of Radiation Medicine and Protection, School for Radiological and Interdisciplinary Sciences (RAD-X), and Collaborative Innovation Center of Radiation Medicine of Jiangsu Higher Education Institutions, Soochow University, Suzhou 215123, China
[c] College of Chemistry, Sichuan University, Chengdu 610065, China

ARTICLE INFO

Keywords:
Uranium
Photocatalysis
Metal-organic framework
Extraction
Post-synthesis

ABSTRACT

Uranium enrichment is perhaps the most critical chemical process throughout the nuclear fuel cycle including uranium mining, uranium extraction from seawater, used fuel reprocessing and disposal, and environmental contamination remediation. New uranium extraction technology is still highly desirable at current stage, although a variety of extraction methods have been established and developed in the past several decades but all with clear demerits. Herein we present a new uranium extraction strategy with combined ligand complexation and photocatalytic reduction based on postsynthetically functionalized metal-organic frameworks (MOFs). The highly robust and photoactive MOF PCN-222 is modified with phosphono- and amino groups that can capture U (VI) from solution. Upon visible light irradiation, the photo-induced electrons from the MOF host can efficiently reduce U(VI) pre-enriched in MOF, affording neutral uranium species that evacuate the MOF structure and regenerating the active site readily for capturing additional U(VI). This auto-recycled process offers an ultrahigh uranium extraction capacity not limited by the number of adsorption sites and more importantly an extra uranium uptake selectivity over these non-redox-active competing metal cations, and can be utilized for uranium separation over extremely wide uranium concentrations and pH ranges, showing a powerful application potential.

1. Introduction

Nuclear power remains to be the most mature technology that can partially substitute fossil energy and provide low-cost electrical power without greenhouse gas emissions [1–4]. However, uranium used in nuclear reactors currently only comes from the mining and milling process, which has already created a global environmental issue of uranium pollution in natural water systems and soils that attracts tremendous public attention [5,6]. In addition, more than 95% of the mass of the used nuclear fuel is the remaining uranium, giving rise to a significant demand for reprocessing the used fuel to further increase the uranium burning efficiency, because of the upcoming shortage of uranium reserving in terrestrial ores [7,8]. Alternatively, uranium in oceans represents another major resource supply of uranium while uranium extraction from seawater currently faces both scientific and technological barriers to be further developed and commercialized [9,10]. Therefore, searching for new materials and strategies for uranium extraction from aqueous solution would be highly desirable aiming for the sustainable development of nuclear power in a variety of aspects including but are not limited to uranium mining, uranium extraction from seawater, used fuel reprocessing and disposal, radioactive waste water treatment, and environmental contamination remediation.

During the past several decades, many different types of solid adsorbent materials have been established and further developed to extract U(VI) (the predominate valence state of uranium under ambient condition) from aqueous solutions, such as inorganic oxides [11–14], modified activated carbon [1,15–17], layered metal sulfides [18–20] or layered hydroxides [21–24], nonporous polymers [25], metal-organic frameworks (MOFs) [26–29], covalent organic frameworks (COFs) [30,31], porous organic polymers (POPs) [2,32], and others [33–37].

* Corresponding authors.
E-mail addresses: zlin@scut.edu.cn (Z. Lin), shuaowang@suda.edu.cn (S. Wang).

https://doi.org/10.1016/j.apcatb.2019.04.087
Received 7 March 2019; Received in revised form 24 April 2019; Accepted 25 April 2019
Available online 26 April 2019

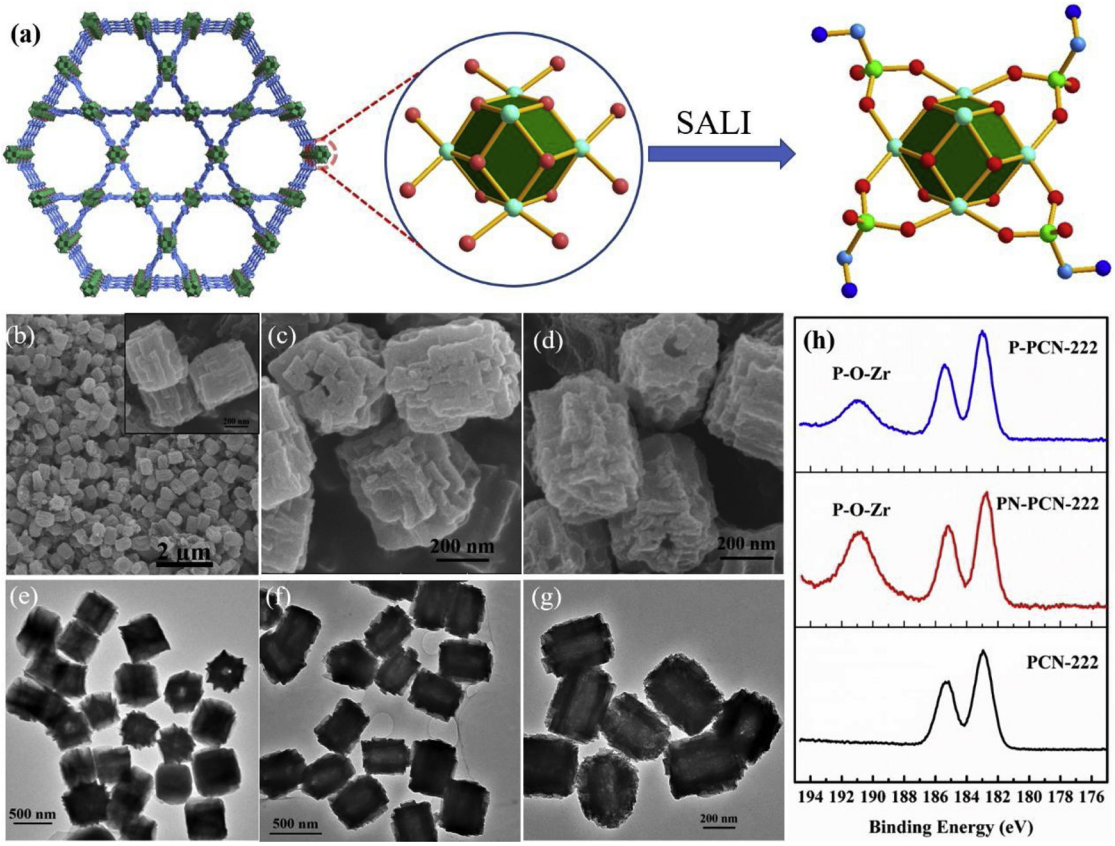

Fig. 1. Schematic representation of SALI (C: Cambridge blue; O: red; N: blue; Zr: green; P: bottle green; H atoms are omitted) (a); SEM images of PCN-222 (b), PN-PCN-222 (c), and P-PCN-222 (d); TEM images of PCN-222 (e), PN-PCN-222 (f), and P-PCN-222 (g); XPS high resolution patterns of Zr(IV) corresponding to PCN-222, PN-PCN-222, and P-PCN-2222 (h), respectively.

However, the U(VI) uptake capabilities of these materials are dramatically affected by solution conditions including temperature, ionic strength, concentrations, pH values, types of coexisting metal cations and complexation ligands *etc.* [38–41]. In a traditional adsorption process, the uptake capacity is predominately determined by the number of adsorption sites, chemical equilibrium between solid and solution, and specific surface area [19,42]. It is therefore a grand challenge to completely eliminate uranium when its initial concentrations are either extremely high or low without additional thermodynamic driving forces. Moreover, competing metal cations such as Ca^{2+} and several transition metal cations often make a great impact on the uranium uptake through competing for the limited active sorption sites in the sorbent [42].

Since U(VI) ion is in general highly soluble and mobile while U(IV) species especially oxides/hydroxides are relatively much more insoluble, reduction of U(VI) to U(IV) followed by precipitation is an alternative and visible approach to separate uranium from aqueous solutions [43,44]. There are a variety of environmentally relevant species reported to be able to reduce U(VI) and have potential applications on uranium sequestration. Systems with zerovalent iron nanoparticles (nano-Fe°), magnetite nanoparticles (nano-Fe_3O_4), ferrous iron, metallic sulfides, and microorganisms in the natural environment have been substantially investigated to be effective in uranyl reduction [43,45–48], however, for these chemical reduction process, the uranium remediation capacity is solely dependent on the amount of reductants while these materials are hardly recyclable. Moreover, nano-Fe° and nano-Fe_3O_4 tend to be efficient in a very narrow pH range and often have a poor reduction selectivity. Theoretically, catalytic reduction is a never-ending process if abundant sacrificial agents are present under the environmentally relevant condition. Semiconductor based photocatalysis has been intensively employed in recent years for hydrogen generation and CO_2 reduction [49–53]. Photocatalytic reduction is a promising technique owing to its high efficiency, reusability of photocatalysts, environmental friendliness, and low energy input if the abundant solar light can be utilized. Although various photocatalysts, such as TiO_2 [54,55], g-C_3N_4 [56,57], and corresponding composite materials [58,59] were studied as reductants for U (VI). Whilst the selectivity for uranyl was not investigated in these works, the efficiency of sole photo-reduction process of U(VI) is still quite limited.

Metal-organic frameworks (MOFs) consisting of metal ions/clusters and functionalized organic linkers, have appeared as new types of photocatalysis materials originating from their well-defined molecular building blocks, tunable functional groups, and effective active sites [60–62]. MOFs can be postsynthetically modified by functionalization of the metal nodes and/or organic linkers [63–66]. This approach is particularly useful when incorporation of distinct chemical functionalities is challenging or impossible *via* direct synthesis. PCN-222 is an extremely robust MOF, composed of $Zr_6(\mu_3\text{-}O)_4(\mu_3\text{-}OH)_4(H_2O)_4(OH)_4$ clusters and photoactive meso-tetra(4-carboxyphenyl)porphyrin (TCPP) linkers [67]. This configuration contains eight terminal labile coordinating ligands (four coordinated water molecules and four hydroxo ligands) available for post-modification through solvent-assisted ligand incorporation (SALI). Phosphonate has been demonstrated to be a very efficient functional ligand to selectively bind U(VI) and this advantage has been taken in many functional materials for uranyl remediation [68–70].

With all these in mind, for the first time, we postsynthetically modify Zr-clusters in PCN-222 with aminomethylphosphonic acid (PN-PCN-222) and ethanephosphonic acid (P-PCN-222), targeting at simultaneous selective complexation and photocatalytic reduction of U (VI) under visible light irradiation. The uranium uptake results reveal

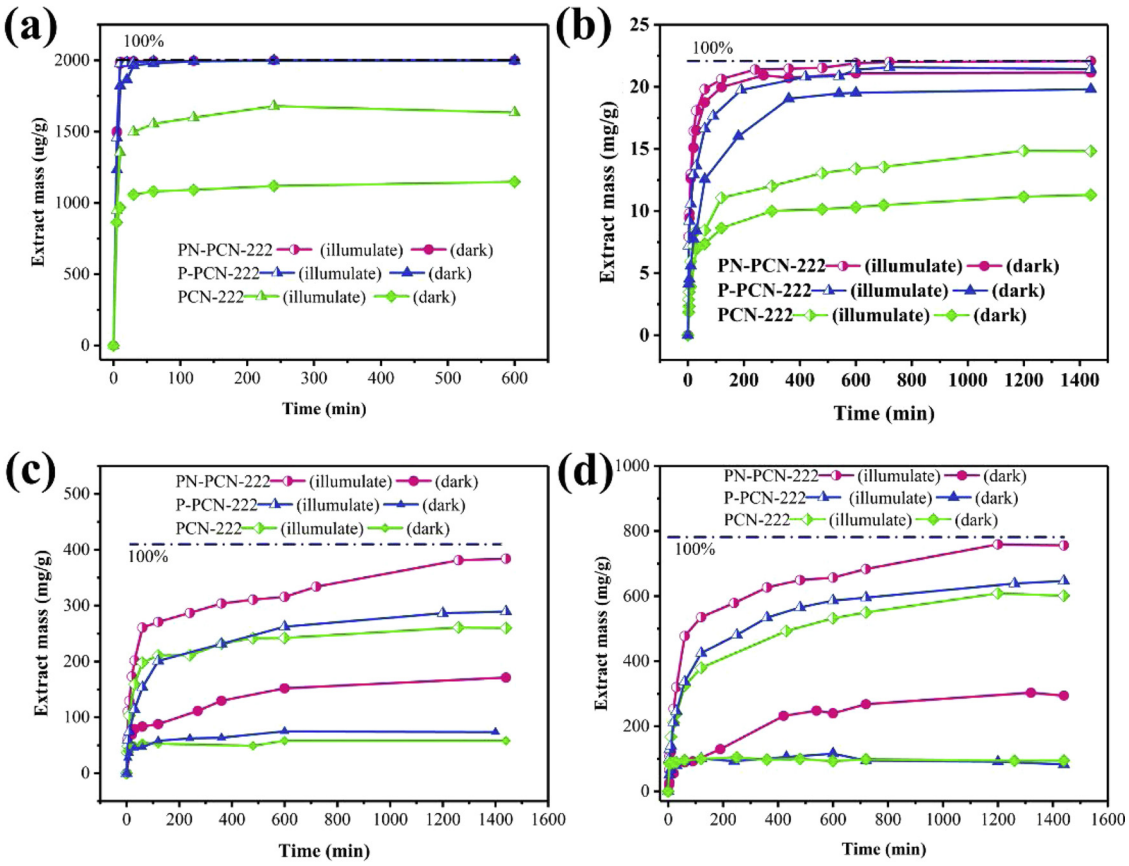

Fig. 2. Uranium extraction by PCN-222, P-PCN-222 and PN-PCN-222 using the photocatalytic reduction method compared to the adsorption method in the dark with initial uranium concentrations of ~1 ppm (a), ~10 ppm (b), ~200 ppm (c), and ~400 ppm (d). m/V = 0.5 g/L, V_{H2O}:V_{CH3OH} = 9:1, N_2 atmosphere, λ ≥ 420 nm.

that uranyl ions can be completely removed with an extremely wide uranyl concentrations range in solution and the uptake amount of uranium reaches 1289 mg/g without saturation, a record high value reported for a MOF material and showing clear advantages in terms of uptake capacity and selectivity over traditional uranium sorbent materials and reductive materials.

2. Experimental

2.1. Materials characterization

Zirconium(IV) chloride ($ZrCl_4$), *N,N*-dimethylformamide (DMF) and benzoic acid were purchased from Aladdin Industrial Inc. Aminomethylphosphonic acid and ethanephosphonic acid were obtained from TCI Chemical Reagent Co., Ltd. Metal salts and nitric acid (trace metal grade) were purchased from Sigma-Aldrich. All commercial chemicals were used without further purification unless otherwise mentioned.

Powder X-ray diffraction (PXRD) patterns were measured on a Bruker D8 advance X-ray diffractometer with Cu K*α* radiation. Synchrotron radiation X-ray diffraction were collected at BL14B1 of Shanghai Synchrotron Radiation Facility (SSRF, China) in transmission mode. The morphology of the products was characterized by field-emission scanning electron microscope (FESEM; Hitachi S-4800) and transmission electron microscope (TEM, JEOL, JEM-1400). A Quantachrome Autosorb Gas Sorption analyzer IQ2 was used to record Brunauer–Emmett–Teller (BET) specific surface area of photocatalysts and all of the samples were degassed at 120 °C before analysis. The UV–vis absorption spectra were recorded on a Shimadzu UV-2401PC spectrophotometer and a white standard of $BaSO_4$ was used as a reference. Infrared spectra were collected on a Thermo Scientific Nicolet iS50 FT-IR instrument at 300 K. X-ray photoelectron spectroscopy (XPS) of the PCN-222, P-PCN-222, PN-PCN-222 and photocatalytic reduction products of U(VI) were performed on ground powders using a Thermo Scientific ESCALAB 250 Xi spectrometer equipped with a monochromatic Al K*α* X-ray source. Cyclic Voltammetry (CV) electrochemical analyzer CHI 660E electrochemical workstation (Chenhua, Shanghai, China) in a conventional three electrodes configuration with working electrode, counter electrode, and reference electrode. The working electrodes prepared with samples have an active area of 1 cm^2 (5 mg), Pt wire and Hg/Hg_2Cl_2 (saturating KCl) were used as the counter electrode and reference electrode, respectively. Mott-Schottky measurements were carried out using Zennium IM6 (Zahner, Germany) in Na_2SO_4 aqueous solution (0.2 M). A 300 W Xe lamp equipped with an ultraviolet cutoff filter (≥ 420 nm) was utilized as the visible light source. The integrated visible light intensity measured with a visible light radiometer was 25 mW/cm^2. The concentrations of metal ions in the filtered solution were determined using inductively coupled plasma-atomic emission spectroscopy (ICP-OES) or inductively coupled plasma-mass spectroscopy (ICP-MS) depending on the uranium concentrations.

2.2. Preparation of PCN-222, PN-PCN-222 and P-PCN-222

Nanoscale PCN-222 was prepared by the solvothermal method according to the published procedure [60]. In a typical synthesis reaction, 20 mg $ZrCl_4$, 500 mg benzoic acid and 400 μL H_2O were added to 4 mL DMF under magnetic stirring. 20 mg TCCP was further dissolved in the above-mentioned solution and kept magnetic stirring for another 10 min. at 300 K. The resulting homogeneous solution was transferred to a 20 mL head space bottle and sealed tightly, followed by heating at 120 °C for 24 h. The products were separated *via* centrifugation at 10,000 rpm for 10 min. To activate the sample, the obtained as-

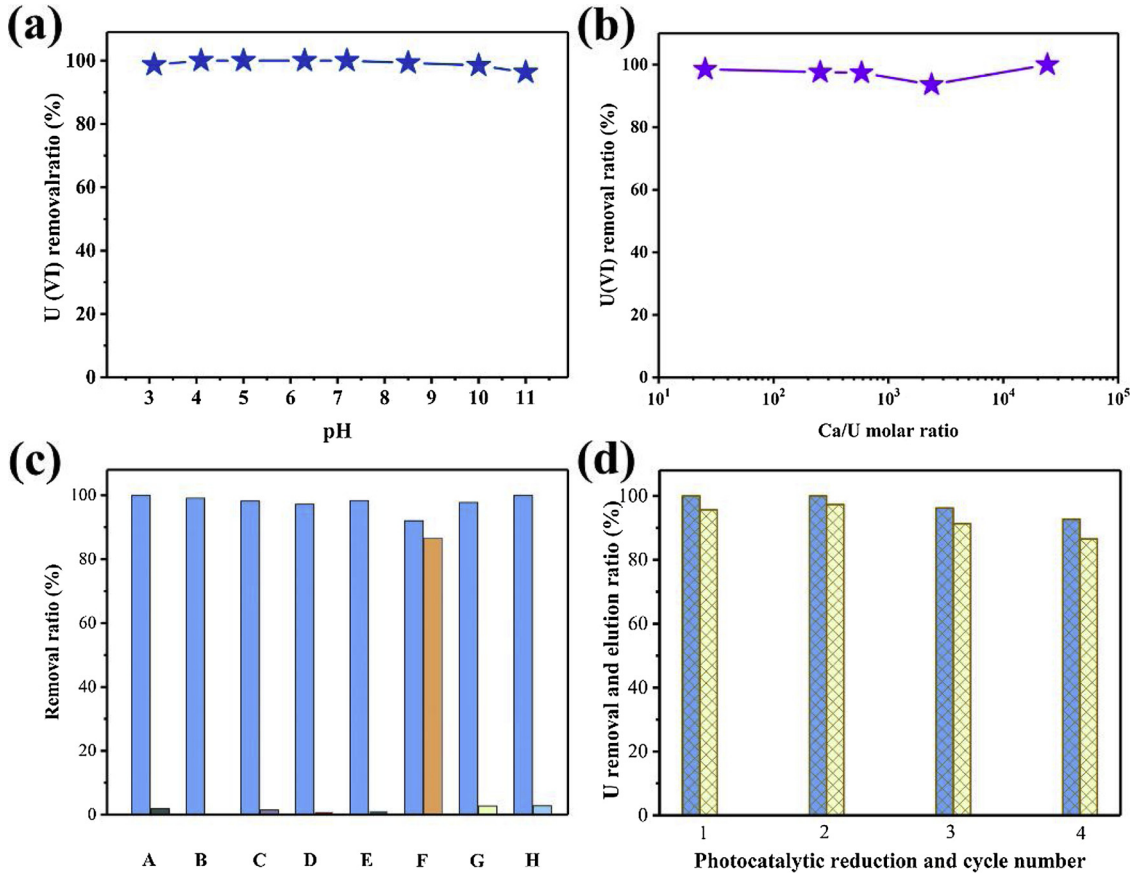

Fig. 3. Extraction efficiency of PN-PCN-222 towards U(VI) at various initial pH values (C_0 in the range of 0.1–5 ppm for U) (a), relative amounts of U removed (%) with the Ca/U molar ratio by photocatalytic reduction (b), extraction efficiency of U and other competing ions (A: U/Mg^{2+}, B: U/Sr^{2+}, C: U/Zn^{2+}, D: U/Co^{2+}, E: U/Cu^{2+}, F: U/Fe^{3+}, G: U/Al^{3+} and H: U/Eu^{3+}, U/M^{n+} = 1:50) by photocatalytic reduction using 10 ppm of U (c) and extraction efficiency of U using photocatalytic reduction method (left axis) and elution efficiency using 0.1 M HCl (right axis) in four cycles (d). $C_0 \approx$ 10 ppm, pH = 4.0, m/V = 0.5 g/L, t = 24 h, and T = 300 K.

synthesized PCN-222 was suspended in a solution of 1.5 mL 4 M HCl in 100 ml DMF, stirred at 120 °C for 12 h, and further purified with methanol and acetone for 48 h. The solvent was replaced in every 8 h and the sample was dried at 100 °C for 12 h under vacuum.

To obtain PN-PCN-222 featuring four aminomethylphosphonic acid ligands per Zr_6 node, we proceeded as follows: a 125 mg portion of activated PCN-222 (0.01 mmol) was placed into a 20 mL vial. Subsequently, 10 mL solution of aminomethylphosphonic acid in H_2O (0.02 M) was added to the reaction vial, which was then capped and heated at 60 °C for 24 h with occasional swirling. The reaction mixture was centrifuged and then soaked in fresh solvent, centrifuged, washed sequentially with CH_3OH (5 × 10 mL), acetone (5 × 10 mL), and finally dried in a vacuum oven at 60 °C A similar method was applied to synthesize P-PCN-222 counterpart using ethanephosphonic acid solution.

2.3. Uranium extraction experiment

The as-prepared PCN-222, P-PCN-222, and PN-PCN-222 samples were used as photocatalysts to reduce U(VI) under visible light irradiation and maintain the reduced uranium complex. The kinetic study of photocatalytic reduction of U(VI) was carried out as follows: 50 mg solid sample was added into 100 ml solutions with various concentrations of U(VI) (1 ppm, 10 ppm, 200 ppm, and 400 ppm), which were prepared by dissolving uranyl nitrate ($UO_2(NO_3)_2{\cdot}6H_2O$) into 100 ml mixture of deionized water and methanol (V_w/V_m = 9:1). Visible light was perpendicularly irradiated on the reaction vessel from a 350 W Xe lamp with a 420 nm cutoff filter. Before irradiation, the solution was bubbled with nitrogen for 120 min to remove oxygen to obtain an anaerobic condition. The N_2 purging was maintained until the uranium extraction finished. Similar process was performed on experiments of sorption without illumination for comparison. The amount of uranium uptake by PCN-222, P-PCN-222, and PN-PCN-222 were calculated using the equation as follow:

$$q_t = (C_0 - C_t)V/m$$

where q_t is the amounts of extracted uranium (mg U/g MOFs.); C_0 and C_t are the initial and final concentrations of uranium (ppm, mg L^{-1}) at each time point; V is the volume of the solution (L), and m is the mass of the MOFs (g). The uranium removal efficiency (%) was calculated as $[(C_0 - C_e)/C_0] \times 100\%$.

Experiments studying the pH dependence of U(VI) photocatalytic reduction were also carried out. Solutions of U(VI) with different pH (in the range of 3–11) were prepared. The pH values were achieved by adding HNO_3 or NaOH solution. The initial concentrations of uranium were 0.1–5 ppm. The experiments on pH dependence of U(VI) were studied by batch method at the m/V ratio of 0.5 g/L (m = 50 mg, V = 100 mL), 300 K, and 24 h contacting time. All samples were isolated by filtration and analyzed further.

The photocatalytic reduction experiments of U(VI) (U = 5 ppm) in the presence of excess 0.3 M NaCl or $NaNO_3$, and $CaCl_2$ (Ca/U molar ratios = 25 to 2.4 × 10^4) were carried out using a m/V ratio of 0.5 g/L and a contacting time of 24 h. Additionally, the performance for uranium extraction in solutions containing 50 times interfering ions, such as Sr^{2+}, Mg^{2+}, Cu^{2+}, Zn^{2+}, Co^{2+}, Fe^{3+}, Al^{3+}, and Eu^{3+}, was evaluated in the same approach.

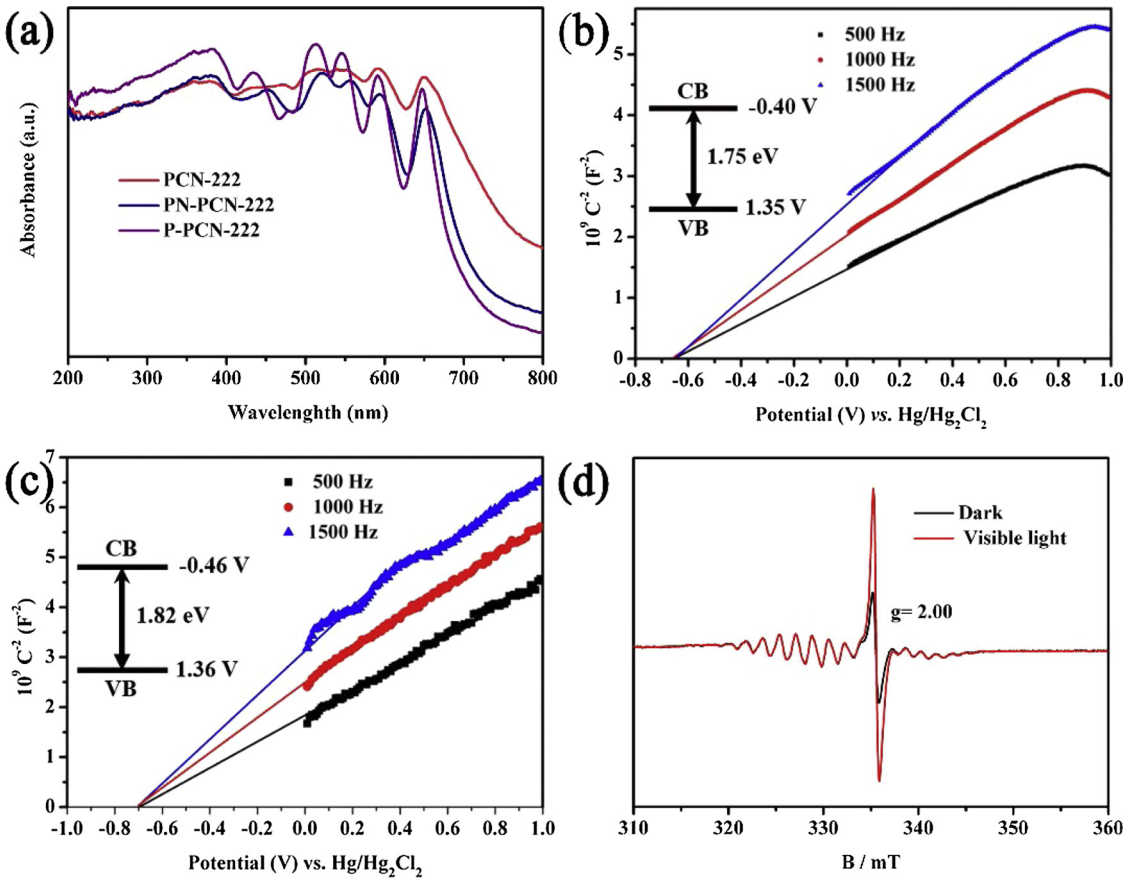

Fig. 4. (a) UV/vis spectra of PCN-222, PN-PCN-222, and P-PCN-222. Mott-Schottky plots for PN-PCN-222 (b) and P-PCN-222 (c) in 0.2 M Na_2SO_4 aqueous solution; inset is the energy diagram of the CB and VB levels, respectively. (d) EPR spectra of PN-PCN-222 in the absence of light (black) and after visible light (400–800 nm) irradiation (red).

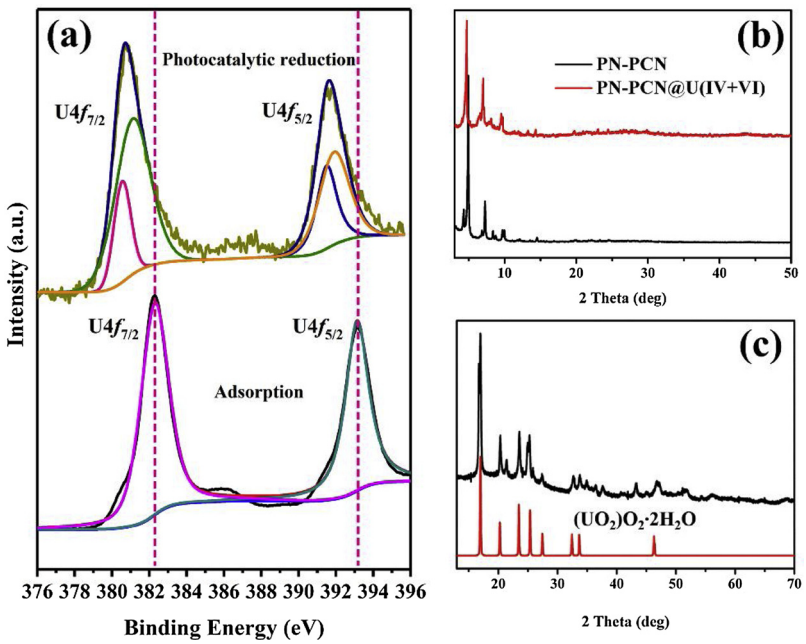

Fig. 5. High-resolution XPS spectra of U 4*f* in photocatalytic reduction and absorption reaction alone (a); PXRD patterns (b) and synchrotron-radiation PXRD pattern of the PN-PCN-222 after 24 h of visible light illumination in a N_2 atmosphere with an initial uranyl concentration of 400 ppm at pH 4 (c) (black: studied sample; red: calculated spectrum of $(UO_2)O_2{\cdot}2H_2O$ (JCPSD 01-081-9033).

3. Results and discussion

PCN-222 is a 3D network based on Zr_6 clusters connected by H_4TCPP ligand and features ultra-large 1D channels of 3.7 nm in diameter [67]. PN-PCN-222 and P-PCN-222 were synthesized through post-synthesis technique by a simple solvent-assisted ligand incorporation (SALI) based on the ligand-exchangeable nature of H_2O and $-OH$ on $Zr_6(\mu_3\text{-}O)_4(\mu_3-OH)_4(H_2O)_4(OH)_4$ clusters (Fig. 1a). The morphology of the as-synthesized PCN-222, PN-PCN-222 and P-PCN-222 were characterized by scanning electron microscopy (SEM) and

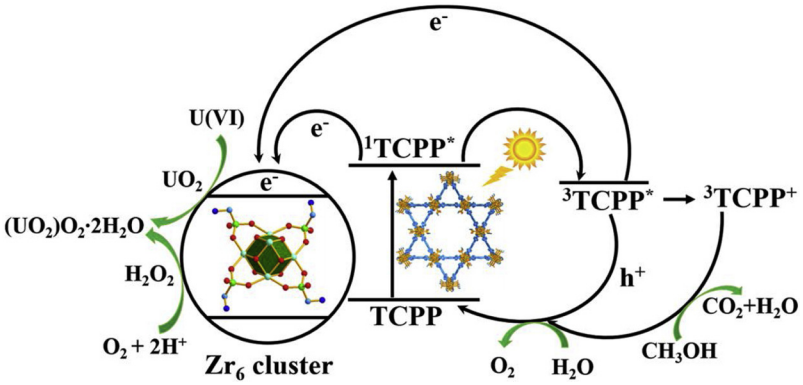

Fig. 6. Schematic illustration of selective enrichment and photocatalytic reduction of U(VI) based on PN-PCN-222.

transmission electron microscopy (TEM). As shown in Fig. 1b–g, the morphologies of the PN-PCN-222 and P-PCN-222 maintain the original hollow nano-tubular habit of PCN-222. The powder X-ray diffraction (PXRD) patterns of the PN-PCN-222 and P-PCN-222 are shown in Fig. S1. The main diffraction peaks match well with the original pattern of PCN-222, suggesting that the original framework structure of PCN-222 retains throughout the modification. The surface area and porosity of PN-PCN-222, P-PCN-222, and PCN-222 were also measured by N_2 adsorption-desorption experiments (Fig. S2). The surface areas of PN-PCN-222 and P-PCN-222 are 608.6 $m^2 g^{-1}$ and 2612.7 $m^2 g^{-1}$, respectively, considerably lower than that of PCN-222 (3315.9 $m^2 g^{-1}$). This is a typical phenomenon due to the occupancy of the channels by the modified ligands for the MOFs [65,66], which paritally blocks the pores. In order to ascertain that the phosphonic acids are successfully grafted onto the Zr clusters chemically rather than the physical adsorption, electron binding energy of Zr in PCN-222, PN-PCN-222, and P-PCN-222 were probed in XPS experiments. As shown in the high-resolution Zr 3*d* spectrum (Fig. 1h), in addition to the binding energy of 182.9 eV and 185.3 eV attributable to Zr $3d_{5/2}$ and $3d_{3/2}$, respectively, in the original spectrum, a brand-new peak emerges at 190.9 eV for PN-PCN-222 and P-PCN-222, which can be assigned to the P-O-Zr bond motif [71,72]. Energy-dispersive X-ray spectroscopy (EDX) was used to evaluate the contents of elements. The corresponding Zr:P molar ratio in PN-PCN-222 and P-PCN-222 both are 1.58, implying that each Zr cluster is coordinated by four organic phosphoric acids, which exactly corresponds to the theoretical maximum modifiable quantity (Fig. S3). This unique type of attachment provides both terminal -NH_2 and unsaturated phosphono- oxygen atom as ligand donors to bind uranyl ion from solution as confirmed below.

To quantitatively evaluate the uranium extraction performance, a series of uptake experiments were conducted, the results of which are shown in Fig. 2. The results reflect the differences in capacity and kinetics with/without photocatalytic reduction. The initial concentrations of uranyl ions are 1 ppm, 10 ppm, 200 ppm, and 400 ppm in the four cases, respectively. In all cases, the total amounts of uranium extracted by PN-PCN-222 and P-PCN-222 are higher than that of PCN-222. It's a solid evidence that the efficiency of uranium extraction is largely enhanced by the SALI induced functional group that shows a high affinity to uranyl ion. For the low concentration cases, uranyl ions can be almost completely removed by both PN-PCN-222 and P-PCN-222 at the solid-liquid ratio (m/V) of 0.5 g/L. Comparatively, only 86.1% and 71.5% of uranyl are removed by PCN-222 under irradiation of visible light, for solutions with initial uranyl concentrations of 1 ppm and 10 ppm, respectively. Meanwhile, 57.3% and 54.5% of uranyl was extracted in the dark reaction (Fig. 2a and b). Under the photocatalytic reduction conditions, there's no uranium removal was observed in the absence of photocatalyst (Fig. S4), indicating that catalyst is indispensable in uranium reduction. The removal percentage differences between irradiation reaction and dark reaction become larger as the initial uranyl concentration increases, especially for PN-PCN-222. Moreover, for initial uranyl concentrations of 200 ppm and 400 ppm, and fixed m/V = 0.5 g/L, uptake in the dark condition shows saturation capacities of 171.4 and 303.5 mg g^{-1}, respectively. In sharp contrast, photocatalytic reductions show no saturation even at the highest initial concentration tested, giving extraction capacities of 381 and 756.1 mg g^{-1}, respectively (Fig. 2c and d). An extraction efficiency of 96.7% is acquired in the photocatalytic reduction for PN-PCN-222 when the initial uranyl concentration is 400 ppm. When reducing the solid-liquid ratio to 0.25 g/L, the uptake amounts are 184.2 and 1289.3 mg/g (Fig. S5), corresponding to the absorption in the dark and photocatalytic reduction, respectively. This extremely high extraction capacity by photocatalytic reduction is approximately seven times higher than that of adsorption. More importantly, nearly all uranyl can be separated by PN-PCN-222 through photocatalytic reduction, regardless of the initial uranyl concentrations (either low or high) (Fig. 2). Note this can not be achieved by adsorption strategy alone. In addition, PN-PCN-222 also exhibits clear advantages compared to P-PCN-222. Extraction rate of photocatalytic reduction for PN-PCN-222 is 96.7%, notably higher than 81.0% and 76.7% for P-PCN-222 and PCN-222, clearly implying the synergistic effect between inner complexation and photocatalytic reductive materials.

Photocatalytic reactions of PN-PCN-222 performed with U(VI) solutions (m/V = 0.5 g/L) of various pH show very high percentages of uranium removal (> 98%) in the pH range of 3.2–7.3 (Fig. 3a, Tab. S1). It is well known that uranyl ion is subject to hydrolysis and precipitation at high pH values in aqueous solution [19]. Therefore, the pH values of the initial solutions with various concentrations of uranium (0.1–5 ppm) were finely controlled to avoid hydrolysis. Even in alkali solutions (the pH range of 8.5–11.2), more than 96% uranyl can be removed. Clearly, PN-PCN-222 is effective in removing uranium under all acidic, neutral, and alkali conditions (pH range of 3.2–11).

Considering uranium mining and milling as well as nuclear accidents would contaminate portable water sources, rivers, and oceans with abundant of competing metal ions, we evaluated the performance of PN-PCN-222 towards uranyl in the presence of large excess of co-existing metal cations. Sodium was chosen to represent of M^+ cations. It was found that the capability of PN-PCN-222 to uranyl removal remains the same despite the surrounding Na^+ is 10^5-fold higher in concentration. Uranyl can be removed completely with the existence of 0.3 M NaCl or $NaNO_3$ even when the concentration of uranyl is low at 5 ppm (Tab. S2). Calcium is considered as a primary competing cation in uranyl removal because it exists extensively in natural water systems, mining water and drinking water in a relatively high concentration, for which $CaCl_2$ was employed to evaluate the impact of Ca^{2+} in our batch experiment. As shown in Fig. 3b and Tab. S3, the removal efficiency and selectivity of PN-PCN-222 towards uranyl keep high although the Ca/U ratio (in mole) is 2.4×10^4, representing a significant improvement over the traditional sorbent materials with ligand complexation or

ion-exchange mechanism only [42,56]. This should be primarily attributed to the selective photocatalytic reduction towards uranyl over these non-redox-active competing cations.

To assess the selectivity and anti-interference PN-PCN-222 in photocatalytic reduction of uranium, the effect of interfering ions including Mg^{2+}, Sr^{2+}, Zn^{2+}, Co^{2+}, Cu^{2+}, Fe^{3+}, Al^{3+}, and Eu^{3+} was investigated separately, which spans over alkaline metals, main group element, transition metals and rare earth elements as well as different valence states (Fig. 3c). The performance of PN-PCN-222 in photocatalytic reduction of uranyl was affirmed to be excellent, as almost all uranyl is removed completely even though the concentration of uranyl is just 5 ppm that's 1/10 of the competing cations and only under the presence of Fe^{3+} the extraction ratio is slightly reduced (Tab. S4). In the case that Fe^{3+} exists, large quantities of photoelectrons are consumed for iron reduction, which affects the reduction of uranium.

Recyclability is another criterium of uranium removal materials, which was also studied in our work. Materials after photocatalytic reduction were soaked in 0.1 M HCl to strip uranium out after being centrifuged from the reaction suspension, which was followed by centrifugation and washed with deionized water and then methanol each for twice as well as dried in vacuum, providing materials for the next round of uranium extraction. The ICP-OES analysis confirms that the removal rate still keeps over 90% and elution efficiency is higher than 80% of initial concentration even though after four photocatalytic reduction-elution cycles (Fig. 3d).

Information about the interaction between uranium and materials can be uncovered by FT-IR spectroscopy (Fig. S6). Obviously, vibration band at 902 cm^{-1} is found in the spectra of PN-PCN-222 before and after light and dark reaction, characteristic for uranyl ion. Additionally, the P—O vibration peak at 991 cm^{-1} for the original sample shifts to 1032 cm^{-1} after uranium uptake while the feature at 1137 cm^{-1} becomes muted, which directly hints for the formation of P—O—U interaction. Moreover, a new peak at 1651 cm^{-1} appears, suggesting the complexation between -NH_2 and U(VI) [68]. These observations confirm the ligand complexation capability for uranyl held by PN-PCN-222.

Semiconductor property of the PCN-222 series materials was characterized to provide insights into the photocatalytic reduction [73,74]. The UV–vis diffuse reflectance spectra of PCN-222, P-PCN-222 and PN-PCN-222 exhibit strong adsorption in the range of 200–800 nm (Fig. 4a), indicating excellent visible light harvesting capabilities. The band gaps of 1.75 eV and 1.82 eV for PN-PCN-222 and P-PCN-222, respectively, can be derived from Tauc plot (Fig. S7). The positive slope in Mott-Schottky plot (C^{-2} *vs* *E*) is consistent with the feature of typical n-type semiconductors. The flat band position was determined to be -0.64 V and -0.70 V *vs* Hg/Hg_2Cl_2 (-0.40 V and -0.46 V *vs* NHE) for PN-PCN-222 and P-PCN-222, respectively. Since the bottom of the conduction band (CB) in n-type semiconductors is approximately equal to the flat-band potential, the CBs of PCN-222 and P-PCN-222 were estimated to be -0.40 V and -0.46 V *vs* NHE and the valence bands (VBs) for both were calculated to be ~1.35 V *vs* NHE (Fig. 4b and c). Because of more negative potential at CBs in PN-PCN-222 and P-PCN-222 than the reduction potential of U(VI) to U(IV) [75], uranyl is theoretically more feasible to be photocatalytically reduced by postsynthesized PCN-222 MOFs than that by PCN-222.

To gain a deeper understanding on the photocatalytic reduction, EPR was used to determine the active intermediates formed during light irradiation (Fig. 4d). Signal at g = 2.003 in EPR spectrum of PN-PCN-222 under dark may be caused by several thermally excited electrons lying in CB [76–78]. This signal is greatly enlarged when the sample is exposed to external irradiation of visible light *in situ*, which confirms the visible-light-induced radical formation on the ligand. Photocatalytic reduction of uranyl occurs only at the Zr_6 oxo cluster, where the catalytic efficiency is determined by the LMCT (ligand-to-metal charge transition) process activated by light-sensitive porphyrin ring itself.

The oxidation states of uranium in the complex produced in photocatalytic reduction was confirmed by XPS analysis. The high-resolution spectra of U $4f_{7/2}$ and U $4f_{5/2}$ shows that the components of produced uranium complex in these MOFs are apparently different between photocatalytic reduction and absorption reaction. (Fig. 5a). In the pattern for the product in the photocatalytic reduction reaction, U $4f_{7/2}$ and $4f_{5/2}$ profiles can be decomposed into two peaks at 380.6 eV, 381.2 eV, and 391.6 eV, 392.0 eV, of which the smaller values signify U (IV) and the large ones correspond to U(VI) [58,59]. However, peaks at 382.3 eV and 393.2 eV are assigned to U(VI) only for produced uranium complex from absorption reaction alone.

The speciation of extracted uranium was further characterized to investigate the photocatalytic reduction extraction mechanism. SEM and TEM images were collected to analyze morphology of the materials after 24 h of uranyl extraction. A small amount of sheets can be found on the surface of materials in the light irradiation system (Fig. S8a) and the cavity becomes opaque (Fig. S8c). The results suggest that the hollow channels in the material were probably filled with solid state uranium compounds. Meanwhile, there's no obvious change on the morphology of PN-PCN-222 before or after both photocatalytic reduction and absorption (Fig. S8). Apart from the unchanged morphology, the intrinsic structural features were also maintained throughout the extraction process (Fig. 5b). In the synchrotron radiation PXRD pattern of sample from photocatalytic reduction, extra peaks in the high-angle region in addition to those of the original sample accord well with those of $(UO_2)O_2{\cdot}2H_2O$ (JCPDS 01-081-9033), which is also known as metastudtite, one of the two naturally occurring uranium peroxide minerals [1,79]. However, in the previous photo or electrochemical characterizations, the uranyl ions were often proposed to be photocatalytically reduced to U(IV) [55,58]. The inconsistency of the reduced species led to further exploration on the photocatalytic reduction process.

To investigate the uranium species, present during the reduction process, the solution chemistry of uranium was characterized electrochemically using cyclic voltammetry (CV). The CV scan curves of uranyl nitrate are shown in Fig. S9. The peaks at -0.35 V (*vs* SCE) of the negative part and 0.1 V (*vs* SCE) of positive part belong to the reduction of U(VI) to U(V) and oxidation of U(V) to U(VI) respectively [54,80]. The U(V) can further disproportionate into U(VI) and U (IV) automatically. This is consistent with the fact that the reduction peak of U(VI) to U(V) has a much greater magnitude than the reverse oxidation peak of U(V) to U(VI) because some of the U(V) transits to U(IV) after formation. Among these three forms of uranium, U(IV) is subject to precipitation, which is further immobilized in the form of UO_2 under the testing condition. The discovery of uranium peroxides was recorded on the surface of UO_2 from nuclear waste and seawater, where the formation of $(UO_2)O_2{\cdot}2H_2O$ was due to the reaction of UO_2 with H_2O_2, a radiolysis product of water [81,82]. In our case, H_2O_2 forms from the photocatalytic reduction of O_2 through electron transfer from triplet porphyrin (^{3}TCPP*). These electrons also react with the captured uranyl, giving both UO_2 and UO_2^+. UO_2^+ further undergoes disproportionation to U(IV) and U(VI); the latter then reacts with H_2O_2 affording $(UO_2)O_2{\cdot}2H_2O$. Nevertheless, either UO_2 or $(UO_2)O_2{\cdot}2H_2O$ are neutral oxide species that can evacuate the MOF host and further free the active sites in MOFs. This is beneficial on facilitating the photocatalytic reduction to ensure a much elevated extraction capacity. Combining all these results, the auto-recycled mechanism is illustrated in Fig. 6.

4. Conclusions

The foregoing results demonstrate a new uranium extraction strategy with combined ligand complexation and photocatalytic reduction achieved by modifying Zr clusters of PCN-222 with ligands showing a high affinity toward uranyl. The obtained PN-PCN-222 is hydrolytically stable for multiple uptake runs and exhibits an elevated uranyl uptake selectivity over the non-redox-active competing metal cations with aid of light irradiation. The amount of extracting uranyl is not limited by the number of absorb sites, and uranyl can be completely

removed from water regardless of the initial uranyl concentrations. This new strategy can overcome several key drawbacks of traditional uranium sorbent materials, whose capabilities can be certainly improved by a systematic search for the combination of photoactive MOF host and complexation ligand in the near future.

Acknowledgements

This work was supported by the National Natural Science Foundation of China (grant no. 21836002, 21825601 and 21777046), the Guangdong Innovative and Entrepreneurial Research Team Program (No. 2016ZT06N569), the China Postdoctoral Science Foundation (no. 2018M633055). The authors thank the beamline BL14B1 (Shanghai Synchrotron Radiation Facility, China) for providing the beam time.

Appendix A. Supplementary data

Supplementary material related to this article can be found, in the online version, at doi:https://doi.org/10.1016/j.apcatb.2019.04.087.

References

[1] C. Liu, P.C. Hsu, J. Xie, J. Zhao, T. Wu, H. Wang, W. Liu, J. Zhang, S. Chu, Y. Cui, Nat. Energy 2 (2017) 17007.
[2] D. Wang, J. Song, J. Wen, Y. Yuan, Z. Liu, S. Lin, H. Wang, H. Wang, S. Zhao, X. Zhao, Adv. Energy Mater. 8 (2018) 1802607.
[3] Y. Yuan, S. Zhao, J. Wen, D. Wang, X. Guo, L. Xu, X. Wang, N. Wang, Adv. Funct. Mater. 29 (2019) 1805380.
[4] S. Chu, A. Majumdar, Nature 488 (2012) 294–303.
[5] H. Lindner, E. Schneider, Energy Econ. 49 (2015) 9–22.
[6] Uranium, Resources, Production, and Demand, OECD Nuclear Energy Agency and the International Atomic Energy Agency, 2014, p. 504 NEA#7209, (2014).
[7] T.P. Lagus, Reprocessing of Spent Nuclear Fuel: A Policy Analysis, 2005, WISE Intern University of Minnesota, 2005.
[8] L.B. Silverio, W. de Queiroz Lamas, Energy Policy 39 (2011) 281–289.
[9] I. Tabushi, Y. Kobuke, T. Nishiya, Nature 280 (1979) 665–666.
[10] R. Davies, J. Kennedy, R. McIlroy, R. Spence, K. Hill, Nature 203 (1964) 1110–1115.
[11] J. Yu, H. Bai, J. Wang, Z. Li, C. Jiao, Q. Liu, M. Zhang, L. Liu, New J. Chem. 37 (2013) 366–372.
[12] J.K. Gao, L.A. Hou, G.H. Zhang, P. Gu, J. Hazard. Mater. 286 (2015) 325–333.
[13] A. Charlot, F. Cuer, A. Grandjean, New J. Chem. 41 (2017) 503–511.
[14] T.M. Budnyak, A.V. Strizhak, A. Gładysz-Płaska, D. Sternik, I.V. Komarov, D. Kołodyńska, M. Majdan, V.A. Tertykh, J. Hazard. Mater. 314 (2016) 326–340.
[15] F. Li, D. Li, X. Li, J. Liao, S. Li, J. Yang, Y. Yang, J. Tang, N. Liu, Chem. Eng. J. 284 (2016) 630–639.
[16] J. Górka, R.T. Mayes, L. Baggetto, G.M. Veith, S. Dai, J. Mater. Chem. A Mater. Energy Sustain. 1 (2013) 3016–3026.
[17] Y. Sun, Z.Y. Wu, X. Wang, C. Ding, W. Cheng, S.H. Yu, X. Wang, Environ. Sci. Technol. 50 (2016) 4459–4467.
[18] M.L. Feng, D. Sarma, Y.J. Gao, X.H. Qi, W.A. Li, X.Y. Huang, M.G. Kanatzidis, J. Am. Chem. Soc. 140 (2018) 11133–11140.
[19] M.L. Feng, D. Sarma, X.H. Qi, K.Z. Du, X.Y. Huang, M.G. Kanatzidis, J. Am. Chem. Soc. 138 (2016) 12578–12585.
[20] M.J. Manos, M.G. Kanatzidis, J. Am. Chem. Soc. 134 (2012) 16441–16446.
[21] R. Li, R. Che, Q. Liu, S. Su, Z. Li, H. Zhang, J. Liu, L. Liu, J. Wang, J. Hazard. Mater. 338 (2017) 167–176.
[22] L. Ma, Q. Wang, S.M. Islam, Y. Liu, S. Ma, M.G. Kanatzidis, J. Am. Chem. Soc. 138 (2016) 2858–2866.
[23] S. Ma, L. Huang, L. Ma, Y. Shim, S.M. Islam, P. Wang, L.-D. Zhao, S. Wang, G. Sun, X. Yang, J. Am. Chem. Soc. 137 (2015) 3670–3677.
[24] Y. Zou, X. Wang, F. Wu, S. Yu, Y. Hu, W. Song, Y. Liu, H. Wang, T. Hayat, X. Wang, ACS Sustain. Chem. Eng. 5 (2017) 1173–1185.
[25] A.J.C. Semião, H.M.A. Rossiter, A.I. Schäfer, J. Membr. Sci. 348 (2010) 174–180.
[26] J. De Decker, J. Rochette, J. De Clercq, J. Florek, P. Van Der Voort, Anal. Chem. 89 (2017) 5678–5682.
[27] J. De Decker, K. Folens, J. De Clercq, M. Meledina, G. Van Tendeloo, G. Du Laing, P. Van Der Voort, J. Hazard. Mater. 335 (2017) 1–9.
[28] T. Zheng, Z. Yang, D. Gui, Z. Liu, X. Wang, X. Dai, S. Liu, L. Zhang, Y. Gao, L. Chen, D. Sheng, Y. Wang, J. Diwu, J. Wang, R. Zhou, Z. Chai, T.E. Albrecht-Schmitt, S. Wang, Nat. Commun. 8 (2017) 15369.
[29] W. Liu, X. Dai, Z. Bai, Y. Wang, Z. Yang, L. Zhang, L. Xu, L. Chen, Y. Li, D. Gui, J. Diwu, J. Wang, R. Zhou, Z. Chai, S. Wang, Environ. Sci. Technol. 51 (2017) 3911–3921.
[30] Y. Yuan, Y. Yang, X. Ma, Q. Meng, L. Wang, S. Zhao, G.S. Zhu, Adv. Mater. 30 (2018) 1706507.
[31] Q. Sun, B. Aguila, L.D. Earl, C.W. Abney, L. Wojtas, P.K. Thallapally, S. Ma, Adv. Mater. 30 (2018) 1705479.
[32] Q. Sun, B. Aguila, J. Perman, A.S. Ivanov, V.S. Bryantsev, L.D. Earl, C.W. Abney, L. Wojtas, S. Ma, Nat. Commun. 9 (2018) 1644.
[33] Y. Yue, R.T. Mayes, J. Kim, P.F. Fulvio, X.G. Sun, C. Tsouris, J. Chen, S. Brown, S. Dai, Angew. Chem. Int. Ed. 52 (2013) 13458–13462.
[34] Z. Pan, D.E. Giammar, V. Mehta, L.D. Troyer, J.G. Catalano, Z. Wang, Environ. Sci. Technol. 50 (2016) 13486–13494.
[35] F. Wu, N. Pu, G. Ye, T. Sun, Z. Wang, Y. Song, W. Wang, X. Huo, Y. Lu, J. Chen, Environ. Sci. Technol. 51 (2017) 4606–4614.
[36] X. Ou, J. Li, Z. Lin, J. Phy. Chem. C 118 (2014) 29887–29895.
[37] Z. Chen, Z. Zhuang, Q. Cao, X. Pan, X. Guan, Z. Lin, ACS Appl. Mater. Interfaces 6 (2014) 1301–1305.
[38] S.E. Crawford, S. Lofts, K. Liber, Environ. Pollut. 220 (2017) 873–881.
[39] H.M. Schulte-Herbrüggen, A.J. Semiao, P. Chaurand, M.C. Graham, Environ. Sci. Technol. 50 (2016) 5817–5824.
[40] C.Z. Wang, J.H. Lan, Q.Y. Wu, Q. Luo, Y.L. Zhao, X.K. Wang, Z.F. Chai, W.Q. Shi, Inorg. Chem. 53 (2014) 9466–9476.
[41] B. Parker, Z. Zhang, L. Rao, J. Arnold, Dalton Trans. 47 (2018) 639–644.
[42] C.W. Abney, R.T. Mayes, T. Saito, S. Dai, Chem. Rev. 117 (2017) 13935–14013.
[43] L. Sheng, J.B. Fein, Environ. Sci. Technol. 48 (2014) 3768–3775.
[44] M.N. Croteau, C.C. Fuller, D.J. Cain, K.M. Campbell, G. Aiken, Environ. Sci. Technol. 50 (2016) 8120–8127.
[45] X. Min, W. Yang, Y.F. Hui, C.Y. Gao, S. Dang, Z.M. Sun, Chem. Commun. (Camb.) 53 (2017) 4199–4202.
[46] I. Pidchenko, K.O. Kvashnina, T. Yokosawa, N. Finck, S. Bahl, D. Schild, R. Polly, E. Bohnert, A. Rossberg, Jr. Göttlicher, Environ. Sci. Technol. 51 (2017) 2217–2225.
[47] E. Calì, J. Qi, O. Preedy, S. Chen, D. Boldrin, W. Branford, L. Vandeperre, M. Ryan, J. Mater. Chem. A Mater. Energy Sustain. 6 (2018) 3063–3073.
[48] L. Ling, X.Y. Huang, W.X. Zhang, Adv. Mater. 30 (2018) 1705703.
[49] Y. Wu, H. Wang, W.G. Tu, Y. Liu, Y.Z. Tan, X.Z. Yuan, J.W. Chew, J. Hazard. Mater. 347 (2018) 412–422.
[50] X.J. Wang, X.L. Zhao, D.Q. Zhang, G.S. Li, H.X. Li, Appl. Catal. B: Environ. 228 (2018) 47–53.
[51] H. Li, S.N. Xiao, J.C. Zhou, J.J. Zhao, F.F. Liu, G.S. Li, D.Q. Zhang, Chem. Commun. (Camb.) 55 (2019) 2741–2744.
[52] Y. Wu, H. Wang, W.G. Tu, S.Y. Wu, Y. Liu, Y.Z. Tan, H.J. Luo, X.Z. Yuan, J.W. Chew, Appl. Catal. B: Environ. 229 (2018) 181–191.
[53] Y. Wu, H. Wang, W.G. Tu, Y. Liu, S.Y. Wu, Y.Z. Tan, J.W. Chew, Appl. Catal. B: Environ. 233 (2018) 58–69.
[54] Y.K. Kim, S. Lee, J. Ryu, H. Park, Appl. Catal. B: Environ. 163 (2015) 584–590.
[55] P. Li, J. Wang, Y. Wang, J. Liang, B. He, D. Pan, Q. Fan, X. Wang, Chem. Eng. J. 365 (2019) 231–241.
[56] C. Lu, P. Zhang, S. Jiang, X. Wu, S. Song, M. Zhu, Z. Lou, Z. Li, F. Liu, Y. Liu, Appl. Catal. B: Environ. 200 (2017) 378–385.
[57] C. Lu, R. Chen, X. Wu, M. Fan, Y. Liu, Z. Le, S. Jiang, S. Song, Appl. Catal. B: Environ. 360 (2016) 1016–1022.
[58] Z.J. Li, Z.W. Huang, W.L. Guo, L. Wang, L.R. Zheng, Z.F. Chai, W.Q. Shi, Environ. Sci. Technol. 51 (2017) 5666–5674.
[59] X.H. Jiang, Q.J. Xing, X.B. Luo, F. Li, J.P. Zou, S.S. Liu, X. Li, X.K. Wang, Appl. Catal. B: Environ. 228 (2018) 29–38.
[60] T. He, S. Chen, B. Ni, Y. Gong, Z. Wu, L. Song, L. Gu, W. Hu, X. Wang, Angew. Chem. 130 (2018) 3551–3556.
[61] A. Schoedel, M. Li, D. Li, M. O'Keeffe, O.M. Yaghi, Chem. Rev. 116 (2016) 12466–12535.
[62] J.P. Zhang, Y.B. Zhang, J.B. Lin, X.M. Chen, Chem. Rev. 112 (2012) 1001–1033.
[63] S.M. Cohen, Chem. Rev. 112 (2012) 970–1000.
[64] T. Islamoglu, S. Goswami, Z. Li, A.J. Howarth, O.K. Farha, J.T. Hupp, Acc. Chem. Res. 50 (2017) 805–813.
[65] M. Taddei, Coord. Chem. Rev. 343 (2017) 1–24.
[66] P. Deria, W. Bury, I. Hod, C.W. Kung, O. Karagiaridi, J.T. Hupp, O.K. Farha, Inorg. Chem. 54 (2015) 2185–2192.
[67] D. Feng, Z.Y. Gu, J.R. Li, H.L. Jiang, Z. Wei, H.C. Zhou, Angew. Chem. 124 (2012) 10453–10456.
[68] Y. Cai, C. Wu, Z. Liu, L. Zhang, L. Chen, J. Wang, X. Wang, S. Yang, S. Wang, Environ. Sci. Nano 4 (2017) 1876–1886.
[69] P. Yang, Q. Liu, J. Liu, R. Chen, R. Li, X. Bai, J. Wang, J. Hazard. Mater. 363 (2019) 248–257.
[70] Y. Cai, L. Chen, S. Yang, L. Xu, H.B. Qin, Z. Liu, L. Chen, X. Wang, S. Wang, ACS Sustain. Chem. Eng. 7 (2019) 5393–5403.
[71] P. Ji, X. Feng, S.S. Veroneau, Y. Song, W. Lin, J. Am. Chem. Soc. 139 (2017) 15600–15603.
[72] C. Garcia-Sancho, J. Cecilia, J. Mérida-Robles, J.S. González, R. Moreno-Tost, A. Infantes-Molina, P. Maireles-Torres, Appl. Catal. B: Environ. 221 (2018) 158–168.
[73] H.Q. Xu, J. Hu, D. Wang, Z. Li, Q. Zhang, Y. Luo, S.H. Yu, H.L. Jiang, J. Am. Chem. Soc. 137 (2015) 13440–13443.
[74] X. Fang, Q. Shang, Y. Wang, L. Jiao, T. Yao, Y. Li, Q. Zhang, Y. Luo, H.L. Jiang, Adv. Mater. 30 (2018) 1705112.
[75] S. Chappa, A.M. Mhatre, V.C. Adya, A.K. Pandey, Appl. Catal. B: Environ. 203 (2017) 53–64.
[76] D. Chen, H. Xing, C. Wang, Z. Su, J. Mater. Chem. A Mater. Energy Sustain. 4 (2016) 2657–2662.
[77] C. Xu, H. Liu, D. Li, J.H. Su, H.L. Jiang, Chem. Sci. 9 (2018) 3152–3158.
[78] Y. Keum, S. Park, Y.P. Chen, J. Park, Angew. Chem. Int. Ed. 57 (2018) 14852–14856.
[79] K.A.H. Kubatko, K.B. Helean, A. Navrotsky, P.C. Burns, Science 302 (2003) 1191–1193.
[80] C. Hennig, A. Ikeda-Ohno, F. Emmerling, W. Kraus, G. Bernhard, Dalton Trans. 39 (2010) 3744–3750.
[81] R.J. Wilbraham, C. Boxall, D.T. Goddard, R.J. Taylor, S.E. Woodbury, J. Nucl. Phys. Mater. Sci. Radiat. Appl. 464 (2015) 86–96.
[82] C. Corbel, G. Sattonnay, S. Guilbert, F. Garrido, M.F. Barthe, C. Jegou, J. Nucl. Phys. Mater. Sci. Radiat. Appl. 348 (2006) 1–17.